ACS APPLIED MATERIALS & INTERFACES

Research Article

www.acsami.org

High Efficiency Inverted Organic Solar Cells with a Neutral Fulleropyrrolidine Electron-Collecting Interlayer

Weidong Xu,[†] Congfei Yan,[†] Zhipeng Kan,[‡] Yang Wang,[†] Wen-Yong Lai,*[,†,§] and Wei Huang[†,§]

[†]Key Laboratory for Organic Electronics and Information Displays (KLOEID) & Institute of Advanced Materials (IAM), Jiangsu National Synergetic Innovation Center for Advanced Materials (SICAM), Nanjing University of Posts & Telecommunications, 9 Wenyuan Road, Nanjing 210023, China

[‡]Physical Sciences and Engineering Division, Solar & Photovoltaic Engineering Research Center (SPERC), King Abdullah University of Science and Technology (KAUST), Thuwal 23955-6900, Saudi Arabia

[§]Key Laboratory of Flexible Electronics (KLOFE) & Institute of Advanced Materials (IAM), Jiangsu National Synergetic Innovation Center for Advanced Materials (SICAM), Nanjing Tech University (NanjingTech), 30 South Puzhu Road, Nanjing 211816, China

Supporting Information

ABSTRACT: A novel fulleropyrrolidine derivative, named FPNOH, was designed, synthesized, and utilized as an efficient electron-collecting (EC) layer for inverted organic solar cells (i-OSCs). The grafted diethanolamino-polar moieties can not only trigger its function as an EC interlayer, but also induce orthogonal solubility that guarantees subsequent multilayer processing without interfacial mixing. A higher power conversion efficiency (PCE) value of 8.34% was achieved for i-OSC devices with ITO/FPNOH EC electrode, compared to that of the sol−gel ZnO based reference devices with an optimized PCE value of 7.92%. High efficiency exceeding 7.7% was still achieved even for the devices with a relatively thick FPNOH film (16.9 nm). It is worthwhile to mention that this kind of material exhibits less thickness dependent performance, in contrast to widely utilized p-type conjugated polyelectrolytes (CPEs) as well as the nonconjugated polyelectrolytes (NCPEs). Further investigation on illuminating intensity dependent parameters revealed the role of FPNOH in reducing interfacial trap-induced recombination at the ITO/active layer interface.

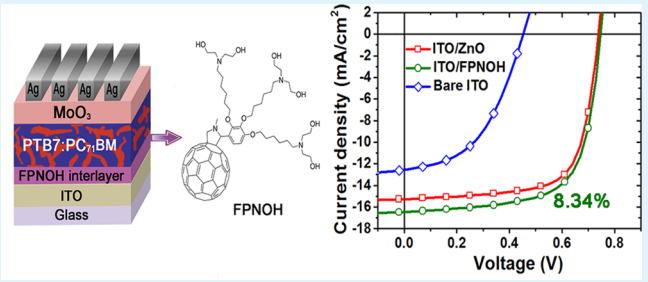

KEYWORDS: *inverted organic solar cells, cathode interlayer, fulleropyrrolidine, electron-collecting, interfacial modification*

1. INTRODUCTION

Inverted organic solar cells (i-OSCs) exhibit superior efficiency and long-term stability compared with the initially implemented conventional device architectures.[1,2] In i-OSCs devices, indium tin oxide (ITO) is not an ideal electron extraction electrode because no quasi-Ohmic contact can form between the photoactive layer and the ITO due to its high work funciton (Φ = 4.7 eV). To reduce the work function of ITO and to improve the electron extractions in i-OSCs, a widely used strategy is to insert an electron-collecting (EC) interfacial layer between the cathode electrode and the photoactive layer. Among all the efforts, inorganic electron selective materials, such as LiF and n-type metal oxides (MOs) (TiO_x, ZnO, MoO_3−Al composite), have been reported as efficient EC layers.[3−6] However, these processes are mostly accompanied by thermal deposition with high vacuum, or solution processing with high temperature annealing treatment, which are not compatible for preparing large-area flexible devices. Alternatively, organic electron selective materials, specifically conjugated polyelectrolytes (CPEs) and nonconjugated polyelectrolytes (NCPEs), have served as an efficient EC interfacial layer because the grafted polar pendants can effectively reduce the work function of ITO electrode as well as the contact resistance, leading to high performance solar cell devices.[7−9] Furthermore, their good film-forming ability and orthogonal solubility provide the potential for large-area processing in roll-to-roll or inkjet printing manufacturing.[10]

Most of the recently explored CPE based EC interlayers were composed of a conjugated polymer backbone, such as polyfluorene,[11,12] polythiophene,[13] and polycarbazole,[14] tethered with numerous polar groups, such as *N*,*N*-dimethylamino,[15,16] ammonium,[17] diethanolamino,[18] and phosphonate.[19] It is worth noting that the widely utilized p-type conjugated backbones are not favorable for electron transport, thus requiring ultrathin film to prevent the possible increased electron extraction barrier.[20] In principle, these p-type polymers, as well as the insulating NCPEs, work as a "dipole" layer to facilitate electron extraction by reducing the Φ of the adjacent electrodes.[21] Although high efficiency could be achieved with these ultrathin films, it is still difficult to ensure

Received: April 4, 2016
Accepted: May 20, 2016
Published: May 20, 2016

DOI: 10.1021/acsami.6b03974
ACS Appl. Mater. Interfaces 2016, 8, 14293−14300

the device performance reproducibility, especially for large-area manufacturing.[22] Moreover, conjugated polymers face the great challenge of batch to batch variations in terms of molecular weight and polydispersity, which may have a significant influence on preparation conditions, such as thickness, solubility, and film morphology.[23]

Fullerene derivatives functionalized with polar pendents are emerging as novel EC interfacial materials to facilitate electron extraction in OSCs due to the circumvention of the undesirable effects often associated with previous reported interlayers.[24−28] The fullerene based EC interlayer has the following advantages: (i) the well-matched energy level with the LUMO level of a commonly utilized acceptor, i.e., [6,6]-phenyl-C61-butyric acid methyl ester (PCBM), ensures the excellent electron extraction ability; (ii) the deep highest occupied molecular orbital (HOMO) energy level provides excellent hole blocking ability; (iii) the reasonable electron mobility. However, most of the fullerene based interfacial materials were demonstrated only in a conventional architecture, i.e., the EC interfacial layer was deposited onto the active layer, followed by thermally evaporating a high work function electrode.[24−28] As far as we are concerned, their application in inverted geometry is rare. One possible reason is that their amphiphilic solubility might prevent multilayer processing, resulting in the interfacial mixing of different layers. That is to say, the bottom EC interlayer is likely to be damaged by the lipophilic solvents used to deposit the subsequent active layers. One alternative way is to introduce cross-linkable fullerene components, as suggested by Cho et al.[29] Very recently, Liu et al. reported a zwitterionic fullerene interlayer, which was sufficiently robust to endure multilayer solution processing, achieving high efficient i-OSC devices.[30]

In the present study, we provide an alternative way on designing novel efficient fullerene based interlayer for i-OSCs. A neutral fulleropyrrolidine EC interfacial material was synthesized and utilized in i-OSCs with the active blend layer of poly[(4,8-bis(2-ethylhexyloxy)-benzo(1,2-*b*:4,5-*b*′)-dithiophene)-2,6-diyl-*alt*-(4-(2-ethylhexyl)-3-fluorothieno[3,4-*b*]thiophene-)-2-carboxylate-2,6-diyl)]: [6, 6]-phenyl-C71-butyric acid methyl ester (PTB7:$PC_{71}BM$). Diethanolamino groups were introduced to trigger the function as an EC interlayer and induce orthogonal solubility. The chemical structure for the interlayer, the active blends, and the device architecture are shown in Figure 1. Inverted geometry with sol−gel derived ZnO as the EC interlayer was fabricated as reference devices.[4] The fulleropyrrolidine interlayer is incorporated between the active layer and ITO electrode, which leads to a significant enhancement of power conversion efficiency (PCE), meanwhile exhibiting less thickness dependent performance.

2. EXPERIMENTAL DETAILS

Detailed Synthesis Procedures Are as Follows. For 2,3,4-tris(6-bromohexyloxy)benzaldehyde **1**, 2,3,4-trihydroxybenzaldehyde (385.3 mg, 2.5 mmol), tetrabutyl ammonium bromide (483.6 mg, 1.5 mmol), and potassium carbonate (2.0732 g, 15 mmol) were added into a 50 mL two-necked round-bottomed flask and dissolved in acetone (20 mL). 1,6-Dibromohexane (2.3 mL) was added via a syringe, and the mixture was stirred at reflux temperature for 18 h. The crude mixture was extracted into chloroform, and the combined organic layers were dried over anhydrous $MgSO_4$. After removal of the solvent under reduced pressure, the brown oil was obtained. The residue was purified by silica gel column chromatography using ethyl acetate as the eluent to give a brown oil, **1** (602 mg, 37%). ^{1}H NMR

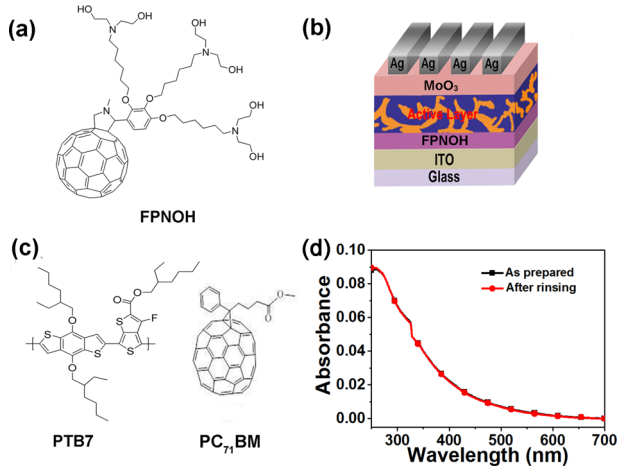

Figure 1. (a) Chemical structures of the neutral fulleropyrrolidine EC interlayer used in solar cell fabrication; (b) the inverted device architecture; (c) the employed active layer components: electron-donor (PTB7) and -acceptor ($PC_{71}BM$) materials; (d) the UV−vis spectra of FPNOH film on quartz before and after chlorobenzene rinsing.

(400 MHz, $CDCl_3$): δ 10.24 (s, 1H), 7.58 (d, J = 8.8 Hz, 1H), 6.72 (d, J = 8.7 Hz, 1H), 4.16 (t, J = 6.6 Hz, 2H), 4.05 (t, J = 6.4 Hz, 2H), 3.98 (t, J = 6.5 Hz, 2H), 3.45−3.40 (m, 6H), 1.94−1.75 (m, 12H), 1.55−1.50 (m, 12H). MALDI-TOF MS (m/z) Calcd for $C_{25}H_{39}Br_3O_4$, exact mass: 640.04. Found: $[M - (2Br)]^+$ 479.95; $[M - Br + Ag]^+$ 668.3.

FPBr. Fullerene-C_{60} (400 mg, 0.56 mmol), sarcosine (92 mg, 1.03 mmol), and **1** (133 mg, 0.21 mmol) were added into a 250 mL two-necked round-bottomed flask. The mixture was flushed with nitrogen, followed by adding 100 mL of deoxygenated 1,2-dichlorobenzene under nitrogen atmosphere. The mixture was stirred at 140 °C for 2 h. The solvent was removed. Then, the mixture was concentrated, and dissolved in chloroform, and the remaining solids were filtered. The resulting filtrate was concentrated and then dissolved in carbon disulfide, purified by silica gel column chromatography using chloroform as the eluent to give a brown solid (141 mg, 49.4%). ^{1}H NMR (400 MHz, $CDCl_3$): δ 7.61 (d, J = 8.8 Hz, 1H), 6.75 (d, J = 8.8 Hz, 1H), 5.35 (s, 1H), 4.97 (d, J = 9.4 Hz, 1H), 4.27 (d, J = 9.4 Hz, 1H), 4.11 (t, J = 6.5 Hz, 2 H), 4.01−3.95 (m, 2H), 3.88 (t, J = 6.6 Hz, 2H), 3.45−3.34 (m, 6H), 2.79 (s, 3H), 1.93−1.87 (m, 3H), 1.80 (d, J = 12.5, 7.2 Hz, 6H), 1.59−1.48 (m, 12H), 1.38 (t, J = 4.2 Hz, 3H). ^{13}C NMR (100 MHz, $CDCl_3$): δ 156.75, 155.06, 154.20, 154.08, 152.92, 152.53, 147.32, 147.30, 147.04, 146.71, 146.34, 146.27, 146.22, 146.19, 146.10, 146.08, 145.97, 145.96, 145.74, 145.60, 145.58, 145.53, 145.33, 145.26, 145.24, 145.10, 144.61, 144.58, 144.44, 144.38, 143.10, 143.04, 142.68, 142.65, 142.62, 142.57, 142.31, 142.26, 142.24, 142.17, 142.12, 142.06, 141.99, 141.89, 141.70, 141.65, 141.58, 141.23, 140.19, 140.12, 139.45, 139.36, 136.57, 136.47, 135.88, 134.70, 124.34, 122.69, 108.64, 73.58, 73.01, 69.97, 69.17, 68.40, 40.15, 33.96, 33.82, 33.72, 32.87, 32.78, 32.68, 30.36, 29.78, 29.70, 29.25, 28.13, 28.05, 27.94, 25.55, 25.36, 25.29. MALDI-TOF MS (m/z) Calcd for $C_{87}H_{44}Br_3NO_3$, exact mass: 1387.09. Mol wt: 1391. Found: 1389.4. Anal. Calcd for $C_{87}H_{44}Br_3NO_3$, C, 75.12; H, 3.19; O, 3.45; N, 1.01. Found: C, 75.02; H, 3.23; O, 3.50; N, 0.97.

FPNOH. FPBr (100 mg) was dissolved in $CHCl_3$ (10 mL) and DMF (5 mL) mixed solvents, and then diethanolamine (1 mL) was added. The mixture was then irradiated at 200 W (75 °C) in cooling mode for 1 h in CEM microwave cavity. After the solvent was evaporated, water was added to get brown solid. The crude powders were washed by methanol and chlorobenzene. Finally, they were moved into a vacuum oven, and kept at 60 °C overnight (98 mg, 94%). ^{1}H NMR (400 MHz, $CDCl_3$): δ 7.60 (d, J = 8.7 Hz, 1H), 6.75 (d, J = 8.8 Hz, 1H), 5.35 (s, 1H), 4.97 (d, J = 9.5 Hz, 1H), 4.26 (d, J = 9.3 Hz, 1H), 4.10 (t, J = 6.8 Hz, 2H), 3.97 (d, J = 9.5 Hz, 2H), 3.89−3.85 (m, 2H), 3.61−3.56 (m, 12H), 2.82 (s,3H), 2.63−2.58 (m, 12H),

DOI: 10.1021/acsami.6b03974
ACS Appl. Mater. Interfaces 2016, 8, 14293−14300

Scheme 1. Synthetic Procedures for FPNOH

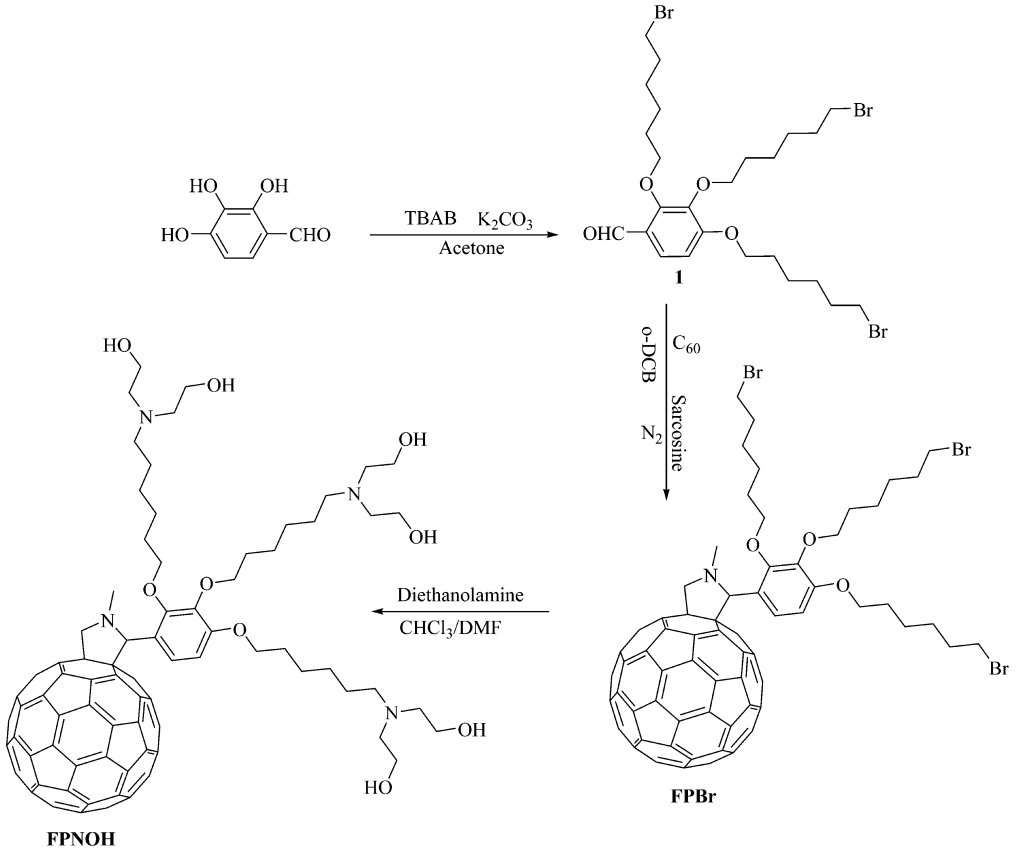

2.54−2.49 (m, 6H), 1.87−1.69 (m, 6H), 1.65−1.57 (m, 3H), 1.54−1.44 (m, 9H), 1.40−1.33 (m, 6H). Anal. Calcd for $C_{99}H_{74}N_4O_9$: C, 81.24; H, 5.10; N, 3.83; O, 9.84. Found: C, 80.94; H, 5.13; N, 4.01; O, 9.92.

Instruments and Measurements. ^{1}H and ^{13}C NMR spectra were recorded on a Bruker Ultra Shield Plus at 400 or 100 MHz, respectively. Mass spectrometry (MS) data of compounds were obtained on a Bruker matrix-assisted laser desorption/ionization time-of-flight mass spectrometry (MALDI-TOF MS) with *trans*-2-[3-(4-*tert*-butylphenyl)-2-methyl-2-propenylidene]malononitrile (DCTB) as the matrix. The UV−vis absorption and transmittance spectra were recorded using a Shimadzu UV-3600 UV−vis−NIR spectrophotometer. Atom force microscopy (AFM) measurements of surface morphology were conducted on the Bruker ScanAsyst AFM in tapping mode. Water contact angles were measured with a CAM 200 (KSV Instrument LID), and the photos were taken with a BASLER A602f-2 camera. The electrochemical behavior of FPNOH and FPBr films were investigated by cyclic voltammetry (CV) with a standard three-electrode electrochemical cell in a 0.1 M tetra-*n*-butylammonium hexafluorophosphate (Bu_4NPF_6) in acetonitrile at room temperature under nitrogen with a scanning rate of 100 mV/s. A platinum working electrode, a platinum wire counter electrode, and a reference electrode of Ag/$AgNO_3$ (0.1 M) were used. The films of fullerene materials for electrochemical measurements were drop-coated from their dilute solution. The LUMO level was determined by the reduction onset. Ferrocene was utilized as the reference.

Fabrication and Characterization of *i*-OSCs. The i-OSC devices were fabricated with a configuration of ITO/FPNOH/active layer/MoO_3/Ag. ITO substrates were precleaned with deionized water, acetone, and isopropanol by ultrasonicating for 15 min each. The substrates were blown dry under a nitrogen stream and immediately exposed to O_2 plasma for 10 min. The sol−gel derived ZnO films were prepared according to the literature.[4] The sol−gel ZnO was spin-cast on ITO substrates with 4000 rpm, followed by annealing in ambient atmosphere at 130 °C for 30 min. The substrates coated with ZnO were then transferred into a nitrogen-filled glovebox (<0.1 ppm of O_2 and H_2O). The FPNOH interlayer was coated in a glovebox to prevent the possible oxygen induced "light soaking" issue.[31] The FPNOH films were cast from their DMF:HOAc (97:3, volume ratio) solutions with various concentration and spin-coating rates, followed by annealing at 100 °C for 15 min to remove DMF residues. The active layer was prepared by spin-coating a mixture of PTB7:$PC_{71}BM$ in chlorobenzene (13 mg/mL for PTB7, 17 mg/mL for $PC_{71}BM$) solution with 3% (volume ratio) 1,8-diiodooctane (DIO) at 3000 rpm for 30 s. After spin-casting, the as-prepared films were covered by a Petri dish in the glovebox for 2 h and then put in vacuum for 30 min. Finally, isopropanol was used to wash DIO residue.[32] Top electrodes were thermally evaporated through a shadow mask onto the active layer. Specifically, the 8.0 nm MoO_3 followed by 80 nm Ag top electrodes were thermally deposited in vacuum at a base pressure of 3 × 10^{-6} Torr. The device architecture for single carrier devices was ITO/FPNOH (or not)/PTB7:$PC_{71}BM$/LiF/Ag. The thickness of evaporated LiF was 1 nm. All the devices were encapsulated in the glovebox with the mixture of epoxy and hardener (1:1 in volume) and then covered with a glass slide. The active area of the pixels as defined by the overlap of anode and cathode area was 0.096 cm^2. Four individual devices were simultaneously prepared on each substrate.

The current density−voltage (*J*−*V*) characteristics were measured by a Keithley 2400 source measure unit. The photocurrent was measured under AM 1.5G illumination at 100 mW/cm^2 using a Newport Thermo Oriel 91192 1000 W Solar Simulator. External quantum efficiency (EQE) spectra were recorded using the monochromated (Bentham) output from a tungsten halogen lamp calibrated with a Newport UV-181 photodiode; phase sensitive detection with a lock-in amplifier was used to increase signal-to-noise.

3. RESULTS AND DISCUSSION

The synthetic procedures of FPNOH are shown in Scheme 1. FPBr, which served as the precursor for FPNOH, was prepared

DOI: 10.1021/acsami.6b03974
ACS Appl. Mater. Interfaces 2016, 8, 14293−14300

by connecting the tris(6-bromohexyloxy)phenyl group through a pyrrolidine ring onto C_{60}. The purified precursor was treated with diethanolamine in a sealed vessel under microwave (MW) irradiation at 75 °C for 60 min (CEM Discover system) in cooling mode, followed by washing with methanol and chlorobenzene (CB). The FPNOH product is insoluble in toluene, CB, and *o*-dichlorobenzene (*o*-DCB), but it is partly dissolved in chloroform (about 3 mg/mL). In contrast, dimethylformamide (DMF) appears to be a good solvent for FPNOH, and the solubility can be improved by adding a small amount of acetic acid (3%, volume ratio) into the solution. To certify their orthogonal-solvent properties, the optical absorption spectra of these interlayer films before and after rinsing with CB were recorded. As shown in Figure 1d, the absorption spectra show no variations, indicating that it will not be damaged by the CB solvent that is commonly used to deposit the subsequent active layer.

The electrochemical properties of the FPNOH were studied by cyclic voltammetry (CV) method, and the corresponding reductive CV curves are shown in Figure 2. Ferrocene was

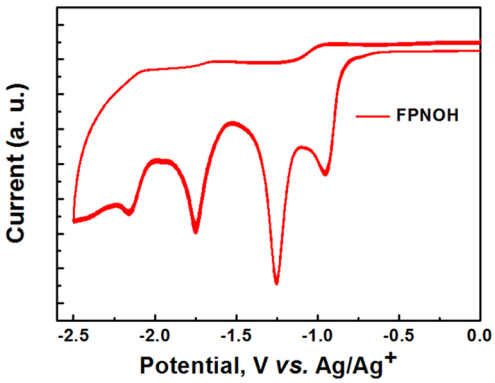

Figure 2. Reductive CV plots of a FPNOH thin film were measured with 0.1 M Bu_4NPF_6 as electrolyte in acetonitrile at a scan rate of 100 mV s^{-1}.

utilized as the reference. FPNOH exhibited three well-defined reduction processes in the scanning range from 0 to −2.5 V. The onset potential for the first reduction was evaluated to be −0.85 V. The calculated LUMO level of FPNOH was around −3.78 eV, which was well-aligned with the LUMO energy level of $PC_{71}BM$ (ranging from −3.7 to −4.3 eV as reported in the literature),[33,34] suggesting the great potential as efficient EC interlayer for FPNOH. Moreover, the absorption onset, determined by UV−vis absorption spectra of FPNOH in films, was equal to 1.80 eV. Thus, the calculated HOMO of FPNOH was −5.58 eV. For comparison, the reductive CV curves for the precursor (FPBr) were also investigated as shown in Figure S1 (Supporting Information, SI). The calculated LUMO level for FPBr was 3.80 eV. The quite similar LUMO level of FPNOH relative to that of its precursor indicates that the different pendent groups in FPBr and FPNOH did not significantly impact the electrochemical properties.

In order to investigate the interfacial properties of FPNOH and the resulting electrodes, water contact angle (θ) measurements were performed on FPNOH-coated (5 mg/mL with a spin speed of 1000 rpm) ITO surfaces in comparison to those of the bare ITO (Figure S2). The bare ITO was largely hydrophilic with a water contact angle of ∼28°. Different from most diethanolamino-functionalized conjugated macromolecules with amphiphilic properties reported in previous literature,[35,36] the resulting diethanolamino-functionalized fullerene derivative FPNOH presented a hydrophobic surface with a water contact angle of ∼95°, which could be attributed to the strong hydrophobic fullerene components.

As shown in Figure 3, the topographic photos for ITO/FPNOH electrode and ITO/FPNOH/PTB7:$PC_{71}BM$ were

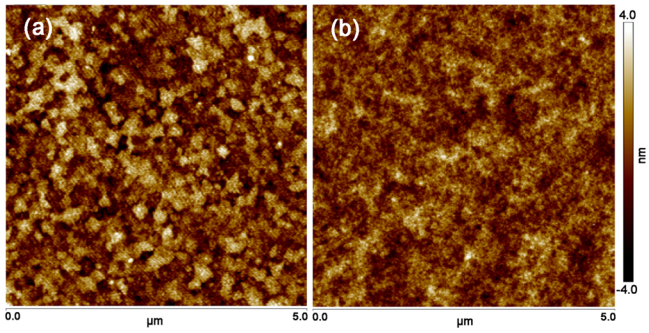

Figure 3. AFM surface topography of (a) FPNOH on ITO and (b) PTB7:$PC_{71}BM$ on ITO/FPNOH. Scan size is 5 μm × 5 μm, and scan rate is 1 Hz for all images. The solution concentration for FPNOH was 5 mg/mL in DMF:HOAc (97:3, volume ratio).

investigated by atomic force microscopy (AFM). For comparison, the AFM topography for bare ITO, ITO/ZnO, and ITO/ZnO/PTB7:$PC_{71}BM$ surfaces are shown in Figures S3 and S4 in SI. The deposited FPNOH with optimized thickness for device fabrication can barely affect the morphology of the bottom electrodes which is similar to previous studies on CPEs and well-defined conjugated macroelectrolyte based interlayers.[23,31] The roughness and topography of the interlayer film are predominantly influenced by ITO electrodes. Nevertheless, the root-mean-square (rms) roughness changed from 2.48 nm for bare ITO to 1.03 nm after FPNOH deposition, which was even smoother than that of the ITO/ZnO film (1.52 nm). It indicated that the introduction of FPNOH can make the bottom surface become smoother before the active layer deposition, which is beneficial for the solution-processed fabrication. The following spin-cast active layer onto ITO/FPNOH and ITO/ZnO electrodes showed similar phase separation morphology, with an rms of 0.75 nm for ITO/FPNOH and 0.82 nm for ITO/ZnO, respectively.

Previous reports showed that CPE and NCPE based interlayers (e.g., PFN, PEIE) generally exhibited strong thickness dependent performance.[8,15] One of the possible reasons is that the widely utilized p-type conjugated backbones, such as polyfluorene, polythiophene, and polycarbazole, are not favorable for electron transport, which would introduce an increasing electron extraction barrier with the increment of interlayer thickness. In contrast, fullerene derivative is one kind of well-known electron affinity material, and thus, it is surmised that this would help to reduce the device sensitivity on the interlayer thickness. To confirm this point, we fabricated a series of i-OSC devices with configuration of ITO/FPNOH/PTB7:$PC_{71}BM$/MoO_3/Ag to study the interlayer thickness dependent device performance. The thickness of FPNOH film was determined according to Beers' law, as described in SI. The thickness for FPNOH films was carefully tuned from 6.0 to 16.9 nm by adjusting the solution concentration from 3 to 10 mg/mL. Photocurrent density−voltage (J−V) characteristics under AM 1.5G irradiation (100 mW/cm^2) are shown in Figure

DOI: 10.1021/acsami.6b03974
ACS Appl. Mater. Interfaces 2016, 8, 14293−14300

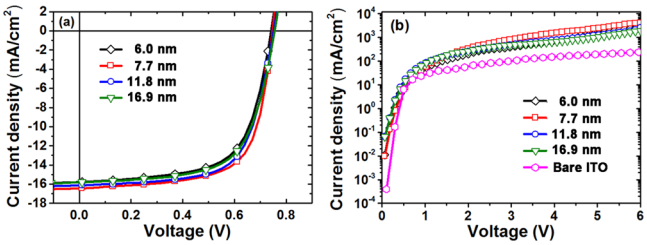

Figure 4. (a) $J-V$ characteristics of solar cells under AM 1.5G irradiation at 100 mW/cm^2 with various FPNOH interlayer thickness; (b) $J-V$ characteristics of the electron-only devices of varying thickness. The device configuration: ITO/interlayer/PTB7:$PC_{71}BM$/LiF/Ag.

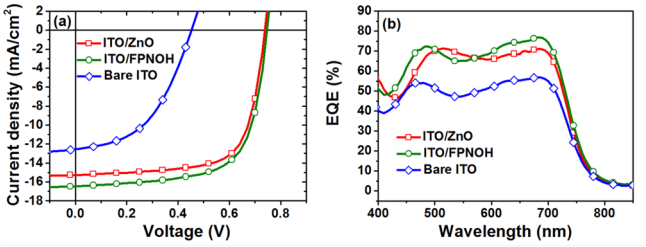

Figure 5. $J-V$ characteristics of solar cells under AM 1.5G irradiation at 100 mW/cm^2 (a) and external quantum efficiency spectra (b) of the inverted devices with ITO/ZnO (□), ITO/FPNOH (○), and bare ITO (◇) cathode.

4a. Detailed device parameters are summarized in Table 1. The maximum PCE value was achieved at 7.7 nm with the concentration of 5 mg/mL at the spin-coating rate of 1000 rpm for 90 s. Increasing the thickness to 16.9 nm would lead to only a slight current loss due to the increase of energy loss during the light across the interlayer or the possible optical spacer effect.[30] For the purpose of demonstrating the ability of FPNOH in reducing the electron extraction barrier as well as investigating the thickness dependent charge transport ability for EC interlayer, the $J-V$ characteristics for electron-only PTB7:$PC_{71}BM$ devices with various FPNOH thicknesses were tested. The device configuration was ITO/FPNOH/PTB7:$PC_{71}BM$/LiF/Ag. For comparison, the devices without FPNOH were fabricated as well. As shown in Figure 4b, the devices based on bare ITO exhibited very low current density, suggesting poor electron injection ability of ITO electrode. After FPNOH deposition, the corresponding single electron devices showed a significant increased current density, suggesting sufficient charge transport ability for ITO/FPNOH electrode. Moreover, the relatively thick film up to 16.9 nm did not lead to an obvious decreased current, which was in line with the i-OSC device results. All these results suggest that the FPNOH EC interlayer shows less thickness dependent performance in contrast to that of previous reported CPEs with p-type conjugated backbones and NCPEs whose devices worked well only with using an ultrathin film (2−8 nm).[9,10,22,23,37]

Next, we fabricated inverted devices with optimal FPNOH spin-casting conditions, and inverted devices with a sol−gel derived ZnO electron extraction layer and bare ITO EC-electrode devices as reference. The representative $J-V$ characteristics of inverted devices with various cathodes (ITO/ZnO, ITO/FPNOH, and ITO) under AM 1.5G irradiation (100 mW/cm^2) are shown in Figure 5a. The main figures of merit of the electrical characterization results are summarized in Table 1. The reference devices without any cathode buffer layer exhibited a very low open circuit V_{OC} of 0.453 V, a short current density (J_{SC}) of 12.51 mA/cm^2, and a fill factor (FF) of 47.5%, giving a maximum PCE of 2.69%. Nevertheless, most of the devices with bare ITO as EC electrode did not work. In the devices with ZnO EC interlayer, a V_{OC} of 0.739 V, a J_{SC} of 15.24 mA/cm^2, and a FF of 70.3% were achieved, leading to a maximum PCE value of 7.92%. The use of optimized FPNOH as an EC interfacial layer (5 mg/mL in DMF/HOAc) resulted in an even higher PCE value of 8.34%, yielding a V_{OC} of 0.747 V, a J_{SC} of 16.42 mA/cm^2, and a FF of 68.0%. In a comparison with bare ITO based devices, the enhancement of V_{OC} could be attributed to the reduced work function of cathode with interlayer deposition.[22] Dark $J-V$ characteristics (Figure S7) verified the good diode behavior of using FPNOH interlayers. Air stability tests on PTB7:$PC_{71}BM$ devices with regular Ca/Al structure and inverted structure with ITO/FPNOH as the cathodes further demonstrated superior device stability for the inverted device with use of FPNOH as the interlayers (Figure S8).

Figure 5b shows the external quantum efficiency (EQE) spectra of the optimized devices. In contrast to the devices based on bare ITO electrode, both ITO/ZnO and ITO/FPNOH based devices exhibited obvious enhancement in their EQE response due to the well-matched work function of the cathode. The EQE value of FPNOH based devices surpasses 70% at around 600−700 nm, indicating an efficient photon-to-electron conversion. They are in line with the values obtained from the $J-V$ characteristics. Transmittance spectra showed that the sol−gel derived ZnO film utilized in i-OSC devices exhibited a much stronger incident light energy loss than FPNOH in the wavelength range 350−500 nm (Figure S5). Consequently, the incorporation of the FPNOH interlayers in i-OSC devices can improve the management of the incident light of 400−500 nm, resulting in higher EQEs.

Table 1. Electrical Parameters of the Inverted Devices with Various Cathodes

cathode	V_{OC}[a] (V)	J_{SC}[a] (mA/cm^2)	FF[a] (%)	best PCE[a] (%)	av PCE[b] (%)
bare ITO	0.453	12.51	47.5	2.69	1.45 ± 1.01
ITO/ZnO	0.739	15.24	70.3	7.92	7.79 ± 0.12
ITO/FPNOH (6.0 nm)	0.742	15.75	64.8	7.57	7.41 ± 0.11
ITO/FPNOH (7.7 nm)	0.747	16.44	68.0	8.34	8.13 ± 0.14
ITO/FPNOH (11.3 nm)	0.752	16.10	66.1	8.00	7.89 ± 0.08
ITO/FPNOH (16.9 nm)	0.755	15.80	64.7	7.73	7.65 ± 0.10

[a]According to the best efficiency of the device. [b]Eight devices in all.

DOI: 10.1021/acsami.6b03974
ACS Appl. Mater. Interfaces 2016, 8, 14293−14300

The light intensity dependent J_{SC} and V_{OC} were further tested to study the bimolecular recombination and interfacial charge traps induced monomolecular recombination in FPNOH based i-OSC devices. The devices based on bare ITO and ITO/ZnO cathodic electrodes were investigated as reference. The results for both J_{SC} and V_{OC} are shown in Figure 6. The equations of fitting power law for both are summarized

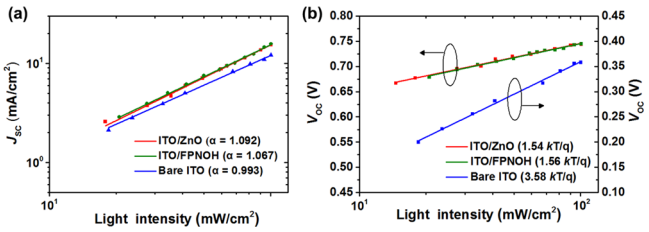

Figure 6. Light intensity dependent J_{SC} (a) and V_{OC} (b), and their corresponding fitting results (line) for i-OSC devices with various cathodes.

in SI. For J_{SC} as a function of illumination intensity, it has been proposed that the deviation for exponent from unity is typically attributed to the bimolecular recombination, space charge effects, and the variations in mobility between the two carriers.[38] The resulting power values (α) were 1.069 for FPNOH based devices, 1.092 for ZnO based devices, and 0.993 for that without the interlayer, suggesting very weak bimolecular recombination at short circuit condition for all the cases, as shown in Figure 6a. The closed α values also indicated that the variations on bottom surface (ITO, ITO/ZnO, and ITO/FPNOH) and roughness did not lead to a large difference on the active layer morphology. The slope of the V_{OC} versus the natural logarithm of the light intensity is often used to describe the competition between bimolecular and monomolecular recombination at open circuit condition.[39] Generally, a stronger light intensity dependent Voc with a slope larger than kT/q could be observed once monomolecular recombination becomes dominant, which is probably induced by interfacial traps.[39] As shown in Figure 6b, the slope for the device with FPNOH is 1.56 kT/q, while a greater slope of 3.58 kT/q for device with bare ITO is observed. The significantly reduced slope with FPNOH deposition can thus be attributed to the reduced trap-assisted recombination at ITO/active layer interface, implying sufficient charge extraction ability of FPNOH EC interfacial layer. The slope for ZnO based device show a close slope value of 1.54 kT/q, suggesting a similar effect in reducing interfacial traps.

The photocurrent density (J_{ph}) versus effective voltage (V_{eff}) curves have been investigated to further understand the exciton dissociation process and the ability of FPNOH in reducing interfacial charge traps.[40,41] Here, $J_{ph} = J_L - J_D$, where J_L and J_D are the current densities under light illumination and in the dark, respectively. $V_{eff} = V_0 - V_a$, where V_0 is the voltage at which $J_{ph} = 0$, and V_a is the applied voltage. The J_{ph}–V_{eff} curves have been shown in Figure 7. For the device with FPNOH interlayer, J_{ph} reaches saturation when the effective voltage V_{eff} arrives at a low voltage around 1 V, which suggested a very weak bimolecular recombination and a very efficient charge collection. In contrast, for the device without the FPNOH interlayer, J_{ph} goes without obvious saturation, which could be attributed to the poor electron extraction ability of the bare ITO.

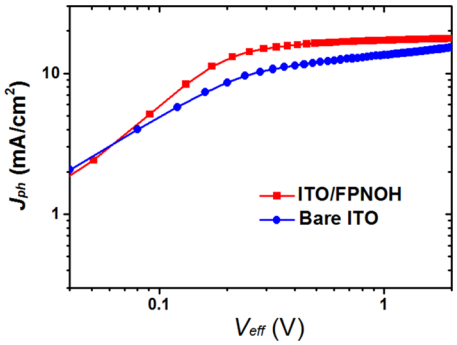

Figure 7. J_{ph}–V_{eff} curves of PTB7:$PC_{71}BM$ devices with or without FPNOH interlayer.

4. CONCLUSION

In summary, we designed and synthesized a neutral full-eropyrrolidine EC interlayer FPNOH for high efficiency i-OSCs with active blends of PTB7:$PC_{71}BM$. Diethanolamino polar groups were introduced to not only trigger its function as an EC interlayer, but also to induce orthogonal solubility that guaranteed subsequent multilayer processing without interfacial mixing. The champion PCE value of 8.34% was achieved, and 3.1-fold enhancement was observed compared with the reference devices based on bare ITO electrode (2.69%). Emphatically, the performance was even higher than that of the devices with sol–gel derived ZnO cathode interlayers (7.92%). On the basis of analysis, FPNOH has the huge advantage of less thickness dependent performance in contrast to previously implemented p-type CPEs based interlayers. According to the study on illuminating the intensity dependence of J_{SC} and V_{OC}, and the photocurrent density versus effective voltage curves, the incorporation of FPNOH as EC interlayers can effectively reduce the interfacial traps and facilitate the charge extraction. The results shed light on rational design and development of high performance EC interlayers with orthogonal solubility and less thickness dependence that would be more compatible with solution based processing techniques, i.e., roll-to-roll or inkjet printing, for manufacturing large-area *i*-OSCs devices.

■ ASSOCIATED CONTENT

Supporting Information

The Supporting Information is available free of charge on the ACS Publications website at DOI: 10.1021/acsami.6b03974.

NMR, MALDI-TOF-MS, optimization of the interlayer thicknesses, and further interface property measurements (PDF)

■ AUTHOR INFORMATION

Corresponding Author

*E-mail: iamwylai@njupt.edu.cn.

Author Contributions

W.X. and C.Y. are both first authors with equal contribution to this work.

Notes

The authors declare no competing financial interest.

■ ACKNOWLEDGMENTS

We acknowledge financial support of the National Key Basic Research Program of China (973 Program, 2014CB648300), the National Natural Science Foundation of China (21422402,

DOI: 10.1021/acsami.6b03974
ACS Appl. Mater. Interfaces 2016, 8, 14293–14300

20904024, 51173081, 61136003), the Natural Science Foundation of Jiangsu Province (BK20140060, BK20130037, BM2012010), Program for Jiangsu Specially-Appointed Professors (RK030STP15001), Program for New Century Excellent Talents in University (NCET-13-0872), Specialized Research Fund for the Doctoral Program of Higher Education (20133223110008, and 20113223110005), the Synergetic Innovation Center for Organic Electronics and Information Displays, the Priority Academic Program Development of Jiangsu Higher Education Institutions (PAPD), the NUPT "1311 Project", the Six Talent Plan (2012XCL035), the 333 Project (BRA2015374), and the Qing Lan Project of Jiangsu Province.

REFERENCES

(1) Lee, K.; Kim, J. Y.; Park, S. H.; Kim, S. H.; Cho, S.; Heeger, A. J. Air-Stable Polymer Electronic Devices. *Adv. Mater.* **2007**, *19*, 2445−2449.

(2) Chen, L. M.; Hong, Z.; Li, G.; Yang, Y. Recent Progress in Polymer Solar Cells: Manipulation of Polymer: Fullerene Morphology and the Formation of Efficient Inverted Polymer Solar Cells. *Adv. Mater.* **2009**, *21*, 1434−1449.

(3) Zhang, F.; Xu, X.; Tang, W.; Zhang, J.; et al. Recent Development of the Inverted Configuration Organic Solar Cells. *Sol. Energy Mater. Sol. Cells* **2011**, *95*, 1785−1799.

(4) Sun, Y.; Seo, J. H.; Takacs, C. J.; Seifter, J.; Heeger, A. J. Inverted Polymer Solar Cells Integrated with a Low-Temperature-Annealed Sol-Gel-Derived ZnO Film as an Electron Transport Layer. *Adv. Mater.* **2011**, *23*, 1679−1683.

(5) Waldauf, C.; Morana, M.; Denk, P.; Schilinsky, P.; Coakley, K.; Choulis, S. A.; Brabec, C. J. Highly Efficient Inverted Organic Photovoltaics Using Solution Based Titanium Oxide as Electron Selective Contact. *Appl. Phys. Lett.* **2006**, *89*, 233517.

(6) Liu, J.; Shao, S.; Fang, G.; Meng, B.; Xie, Z.; Wang, L. High-Efficiency Inverted Polymer Solar Cells with Transparent and Work-Function Tunable MoO_3-Al Composite Film as Cathode Buffer Layer. *Adv. Mater.* **2012**, *24*, 2774−2779.

(7) Duan, C. H.; Zhang, K.; Zhong, C. M.; Huang, F.; Cao, Y. Recent Advances in Water/Alcohol-Soluble π-conjugated Materials: New Materials and Growing Applications in Solar Cells. *Chem. Soc. Rev.* **2013**, *42*, 9071−9104.

(8) Zhou, Y.; Fuentes-Hernandez, C.; Shim, J.; Meyer, J.; Giordano, A. J.; Li, H.; Winget, P.; Papadopoulos, T.; Cheun, H.; Kim, J.; Fenoll, M.; Dindar, A.; Haske, W.; Najafabadi, E.; Khan, T. M.; Sojoudi, H.; Barlow, S.; Graham, S.; Brédas, J.-L.; Marder, S. R.; Kahn, A.; Kippelen, B. A Universal Method to Produce Low-Work Function Electrodes for Organic Electronics. *Science* **2012**, *336*, 327−332.

(9) Nam, S.; Seo, J.; Woo, S.; Kim, W.; Kim, H.; Bradley, D. D. C.; Kim, Y. Inverted Polymer Fullerene Solar Cells Exceeding 10% Efficiency with Poly(2-ethyl-2-oxazoline) Nanodots on Electron-Collecting Buffer Layers. *Nat. Commun.* **2015**, *6*, 8929.

(10) Andersen, T. R.; Dam, H. F.; Hösel, M.; Helgesen, M.; Carlé, J. E.; Larsen-Olsen, T. T.; Gevorgyan, S. A.; Andreasen, J. W.; Adams, J.; Li, N.; Machui, F.; Spyropoulos, G. D.; Ameri, T.; Lemaître, N.; Legros, M.; Scheel, A.; Gaiser, D.; Kreul, K.; Berny, S.; Lozman, O. R.; Nordman, S.; Välimäki, M.; Vilkman, M.; Søndergaard, R. R.; Jørgensen, M.; Brabec, C. J.; Krebs, F. C. Scalable, Ambient Atmosphere Roll-to-Roll Manufacture of Encapsulated Large Area, Flexible Organic Tandem Solar Cell Modules. *Energy Environ. Sci.* **2014**, *7*, 2925−2933.

(11) He, Z. C.; Zhong, C. M.; Su, S. J.; Xu, M.; Wu, H. B.; Cao, Y. Enhanced Power-Conversion Efficiency in Polymer Solar Cells Using an Inverted Device Structure. *Nat. Photonics* **2012**, *6*, 591−595.

(12) Xu, W.; Zhang, X.; Hu, Q.; Zhao, L.; Teng, X.; Lai, W.-Y.; Xia, R.; Nelson, J.; Huang, W.; Bradley, D. D. C. Fluorene-Based Cathode Interlayer Polymers for High Performance Solution Processed Organic Optoelectronic Devices. *Org. Electron.* **2014**, *15*, 1244−1253.

(13) Zilberberg, K.; Behrendt, A.; Kraft, M.; Scherf, U.; Riedl, T. Ultrathin Interlayers of a Conjugated Polyelectrolyte for Low Work-Function Cathodes in Efficient Inverted Organic Solar Cells. *Org. Electron.* **2013**, *14*, 951−957.

(14) Sun, J. M.; Zhu, Y. X.; Xu, X. F.; Lan, L. F.; Zhang, L. J.; Cai, P.; Chen, J. W.; Peng, J. B.; Cao, Y. High Efficiency and High V_{OC} Inverted Polymer Solar Cells Based on a Low-Lying HOMO Polycarbazole Donor and a Hydrophilic Polycarbazole Inter Layer on ITO Cathode. *J. Phys. Chem. C* **2012**, *116*, 14188−14198.

(15) Xia, R.; Leem, D.-S.; Kirchartz, T.; Spencer, S.; Murphy, C.; He, Z. C.; Wu, H. B.; Su, S. J.; Cao, Y.; Kim, J. S.; deMello, J. C.; Bradley, D. D. C.; Nelson, J. Investigation of a Conjugated Polyelectrolyte Interlayer for Inverted Polymer:Fullerene Solar Cells. *Adv. Energy Mater.* **2013**, *3*, 718−723.

(16) Lv, M.; Li, S.; Jasieniak, J. J.; Hou, J.; Zhu, J.; Tan, Z.; Watkins, S. E.; Li, Y.; Chen, X. A Hyperbranched Conjugated Polymer as the Cathode Interlayer for High Performance Polymer Solar Cells. *Adv. Mater.* **2013**, *25*, 6889−6894.

(17) Min, J.; Zhang, H.; Stubhan, T.; Luponosov, Y. N.; Kraft, M.; Ponomarenko, S. A.; Ameri, T.; Scherf, U.; Brabec, C. J. A Combination of Al-Doped ZnO and a Conjugated Polyelectrolyte Interlayer for Small Molecule Solution Processed Solar Cells with an Inverted Structure. *J. Mater. Chem. A* **2013**, *1*, 11306−11311.

(18) Xu, W.; Lai, W.-Y.; Hu, Q.; Teng, X. Y.; Zhang, X. W.; Huang, W. A Hydrophilic Monodisperse Conjugated Starburst Macromolecule with Multidimensional Topology as Electron Transport/ Injection Layer for Organic Electronics. *Polym. Chem.* **2014**, *5*, 2942−2950.

(19) Ye, T. L.; Zhu, M. R.; Chen, J. S.; Fu, Q.; Zhao, F. C.; Shi, C. S.; Hu, Y.; Ma, D. G.; Yang, C. L. Efficient Electron Injection Layer Based on Thermo-Cleavable Materials for Inverted Bottom-Emission Polymer Light Emitting Diodes. *J. Mater. Chem.* **2012**, *22*, 6413−6418.

(20) Liu, Y.; Page, Z. A.; Russell, T. P.; Emrick, T. Finely Tuned Polymer Interlayers Enhance Solar Cell Efficiency. *Angew. Chem., Int. Ed.* **2015**, *54*, 11485−11489.

(21) Chueh, C.-C.; Li, C.-Z.; Jen, A. K.-Y. Recent Progress and Perspective in Solution-Processed Interfacial Materials for Efficient and Stable Polymer and Organometal Perovskite Solar Cells. *Energy Environ. Sci.* **2015**, *8*, 1160−1189.

(22) Liu, S.; Zhang, K.; Lu, J.; Zhang, J.; Yip, H.-L.; Huang, F.; Cao, Y. High-Efficiency Polymer Solar Cells via the Incorporation of an Amino-Functionalized Conjugated Metallopolymer as a Cathode Interlayer. *J. Am. Chem. Soc.* **2013**, *135*, 15326−15329.

(23) Xu, W.; Kan, Z.; Ye, T. L.; Zhao, L.; Lai, W.-Y.; Xia, R.; Lanzani, G.; Keivanidis, P. E.; Huang, W. Well-Defined Star-Shaped Conjugated Macroelectrolytes as Efficient Electron-Collecting Interlayer for Inverted Polymer Solar Cells. *ACS Appl. Mater. Interfaces* **2015**, *7*, 452−459.

(24) Page, Z. A.; Liu, Y.; Duzhko, V. V.; Russell, T. P.; Emrick, T. Fulleropyrrolidine Interlayers: Tailoring Electrodes to Raise Organic Solar Cell Efficiency. *Science* **2014**, *346*, 441−444.

(25) Mei, Q.; Li, C.; Gong, X.; Lu, H.; Jin, E.; Du, C.; Lu, Z.; Jiang, L.; Meng, X.; Wang, C.; Bo, Z. Enhancing the Performance of Polymer Photovoltaic Cells by Using an Alcohol Soluble Fullerene Derivative as the Interfacial Layer. *ACS Appl. Mater. Interfaces* **2013**, *5*, 8076−8080.

(26) Zhang, Z.-G.; Li, H.; Qi, B.; Chi, D.; Jin, Z.; Qi, Z.; Hou, J.; Li, Y.; Wang, J. Amine Group Functionalized Fullerene Derivatives as Cathode Buffer Layers for High Performance Polymer Solar Cells. *J. Mater. Chem. A* **2013**, *1*, 9624−9629.

(27) O'Malley, K. M.; Li, C.-Z.; Yip, H.-L.; Jen, A. K. Y. Enhanced Open-Circuit Voltage in High Performance Polymer/Fullerene Bulk-Heterojunction Solar Cells by Cathode Modification with a C 60 Surfactant. *Adv. Energy Mater.* **2012**, *2*, 82−86.

(28) Yang, X.; Chueh, C.-C.; Li, C.-Z.; Yip, H.-L.; Yin, P.; Chen, H.; Chen, W.-C.; Jen, A. K. Y. High-Efficiency Polymer Solar Cells Achieved by Doping Plasmonic Metallic Nanoparticles into Dual Charge Selecting Interfacial Layers to Enhance Light Trapping. *Adv. Energy Mater.* **2013**, *3*, 666−673.

(29) Cho, N.; Li, C.-Z.; Yip, H.-L.; Jen, A. K. Y. In Situ Doping and Crosslinking of Fullerenes to Form Efficient and Robust Electron-

DOI: 10.1021/acsami.6b03974
ACS Appl. Mater. Interfaces 2016, 8, 14293−14300

Transporting Layers for Polymer Solar Cells. *Energy Environ. Sci.* **2014**, *7*, 638−643.
(30) Liu, Y.; Page, Z.; Ferdous, S.; Liu, F.; Kim, P.; Emrick, T.; Russell, T. Dual Functional Zwitterionic Fullerene Interlayer for Efficient Inverted Polymer Solar Cells. *Adv. Energy Mater.* **2015**, *5*, 1500405.
(31) Xu, W.; Xia, R.; Ye, T. L.; Zhao, L.; Kan, Z.; Mei, Y.; Yan, C.; Zhang, X.-W.; Lai, W.-Y.; Keivanidis, P. E.; Huang, W. Understanding the Light Soaking Effects in Inverted Organic Solar Cells Functionalized with Conjugated Macroelectrolyte Electron-Collecting Interlayers. *Adv. Sci.* **2016**, *3*, 1500245.
(32) Guo, S.; Cao, B.; Wang, W.; Moulin, J.-F.; Müller-Buschbaum, P. Effect of Alcohol Treatment on the Performance of PTB7:PC71BM Bulk Heterojunction Solar Cells. *ACS Appl. Mater. Interfaces* **2015**, *7*, 4641−4649.
(33) Duan, C.; Zhong, C.; Liu, C.; Huang, F.; Cao, Y. Highly Efficient Inverted Polymer Solar Cells Based on an Alcohol Soluble Fullerene Derivative Interlayer. *Chem. Mater.* **2012**, *24*, 1682−1689.
(34) Li, C.-Z.; Yip, H.-L.; Jen, A. K.-Y. Functional Fullerenes for Organic Photovoltaics. *J. Mater. Chem.* **2012**, *22*, 4161−4177.
(35) Huang, F.; Niu, Y.-H.; Zhang, Y.; Ka, J.-W.; Liu, M. S.; Jen, A. K. Y. A Conjugated, Neutral Surfactant as Electron-Injection Material for High-Efficiency Polymer Light-Emitting Diodes. *Adv. Mater.* **2007**, *19*, 2010−2014.
(36) Huang, F.; Zhang, Y.; Liu, M. S.; Jen, A. K. Y. Electron-Rich Alcohol-Soluble Neutral Conjugated Polymers as Highly Efficient Electron-Injecting Materials for Polymer Light-Emitting Diodes. *Adv. Funct. Mater.* **2009**, *19*, 2457−2466.
(37) Ouyang, X.; Peng, R.; Ai, L.; Zhang, X.; Ge, Z. Efficient Polymer Solar Cells Employing a Non-Conjugated Small-Molecule Electrolyte. *Nat. Photonics* **2015**, *9*, 520−524.
(38) Koster, L. J. A.; Kemerink, M.; Wienk, M. M.; Maturová, K.; Janssen, R. A. J. Quantifying Bimolecular Recombination Losses in Organic Bulk Heterojunction Solar Cells. *Adv. Mater.* **2011**, *23*, 1670−1674.
(39) Koster, L. J. A.; Mihailetchi, V. D.; Ramaker, R.; Blom, P. W. M. Light Intensity Dependence of Open-Circuit Voltage of Polymer:-fullerene Solar Cells. *Appl. Phys. Lett.* **2005**, *86*, 123509.
(40) Zhang, M.; Zhang, F.; An, Q.; Sun, Q.; Wang, W.; Zhang, J.; Tang, W. Highly Efficient Ternary Polymer Solar Cells by Optimizing Photon Harvesting and Charge Carrier Transport. *Nano Energy* **2016**, *22*, 241−254.
(41) An, Q.; Zhang, F.; Sun, Q.; Wang, J.; Li, L.; Zhang, J.; Tang, W.; Deng, Z. Efficient Small Molecular Ternary Solar Cells by Synergistically Optimized Photon Harvesting and Phase Separation. *J. Mater. Chem. A* **2015**, *3*, 16653−16662.

DOI: 10.1021/acsami.6b03974
ACS Appl. Mater. Interfaces 2016, 8, 14293−14300